A&A 534, A31 (2011)
DOI: 10.1051/0004-6361/201117461
© ESO 2011

Astronomy & Astrophysics

The complete census of optically selected AGNs in the Coma supercluster: the dependence of AGN activity on the local environment⋆

G. Gavazzi[1], G. Savorgnan[1], and Mattia Fumagalli[2]

[1] Dipartimento di Fisica G. Occhialini, Università di Milano-Bicocca, Piazza della Scienza 3, 20126 Milano, Italy
e-mail: giuseppe.gavazzi@mib.infn.it
[2] Leiden Observatory, Leiden University, PO Box 9513, 2300 RA Leiden, The Netherlands
e-mail: fumagalli@strw.leidenuniv.nl

Received 10 June 2011 / Accepted 18 July 2011

ABSTRACT

Aims. To investigate the dependence of the occurrence of active galactic nuclei (AGNs) on local galaxy density, we study the nuclear properties of ∼5000 galaxies in the Coma supercluster whose density spans two orders of magnitude from the sparse filaments to the cores of rich clusters.

Methods. We obtained optical spectra of the nuclei of 283 galaxies using the 1.5 m *Cassini* telescope of Bologna observatory. Among these galaxies, 177 belong to the Coma supercluster and are added to the 4785 spectra available from SDSS (DR7) to fill-in the incomplete coverage by SDSS of luminous galaxies. We perform a spectral classification of the nuclei of galaxies in this region (with a completeness of 98% at $r \leq 17.77$), classifying the nuclear spectra in six classes: three of them (SEY, sAGN, LIN) refer to AGNs and the remaining three (HII, RET, PAS) refer to different stages of starburst activity. We perform this classification as recommended by Cid Fernandes and collaborators using the ratio of λ 6584 [NII] to Hα lines and the equivalent width of Hα (WHAN diagnostic), after correcting the last quantity by 1.3 Å for underlying absorption.

Results. We find that 482 (10%) of 5027 galaxies host an AGN: their frequency strongly increases with increasing luminosity of the parent galaxies, such that 32% of galaxies with $\mathrm{Log}(L_i/L_\odot) \geq 10.2$ harbor an AGN at their interior. In addition to their presence in luminous galaxies, AGNs are also found in red galaxies with $\langle g-i \rangle \simeq 1.15 \pm 0.15$ mag. The majority of SEY and sAGN (strong AGNs) are associated with luminous late-type (or S0a) galaxies, while LIN (weak AGNs) and RET ("retired": nuclei that have experienced a starburst phase in the past and are now ionized by their hot evolved low-mass stars), are mostly found among E/S0as. The number density of AGNs, HII region-like, and retired galaxies is found to anti-correlate with the local density of galaxies, such that their frequency drops by a factor of two near the cluster cores, while the frequency of galaxies containing passive nuclei increases by the same amount towards the center of rich clusters. The dependence of AGN number density on the local galaxy density is greater than the one implied by morphology segregation alone.

Key words. galaxies: clusters: individual: Coma – galaxies: evolution – galaxies: nuclei

1. Introduction

It appears that 1.5 m class telescopes, especially those ones located in zones of marginal climatic conditions, have lost much of their *raison d'etre*, particularly after the advent of the Sloan Digital Sky Survey (SDSS). They however maintain a crucial didactic value for the training of young astronomers and provided that they are employed for suitable projects, can still make some significant niche contribution. One appropriate project in this respect is, in our opinion, the determination of the spectral properties of nuclei of bright galaxies, as part of a general study to perform a complete census of active galactic nuclei (AGNs). A spectral resolution on the order of $R = 1000$ in the red channel (the blue-arm is more penalized by the relative blindness of CCDs) is sufficient to measure in a matter of a few minutes, even in non-photometric conditions, some crucial line ratios in the nuclear regions of galaxies, owing to their high surface brightness.

In this spirit, one of us (G.G.) invited yearly his first year master students to participate in some observing runs at the 1.5 m Loiano telescope of the Observatory of Bologna (It). Unsurprisingly, many nights were affected by poor weather, although an amazing wealth of nuclear spectra (283) of nearby galaxies was accumulated, suitable for detecting any AGNs harbored in their interior.

A large amount of data (177) were gathered for the region of the Coma supercluster, on which this work is focused. Following a fortunate run of 7/8 photometric nights in spring 2011 and the appearance of Mahajan et al. (2010), who investigated the AGN environmental dependence in the Coma supercluster relying purely on SDSS data, regardless of its well-known incompleteness at the bright end (Blanton et al. 2005a,b,c), we decided to publish our measurements derived in the past six years, with the hope that they might contribute to improving our understanding of AGNs.

There is a clear need to establish the frequency of AGNs of various types, in various environments, locally and in a cosmological perspective, to improve our understanding of galaxy assembly. Nevertheless, even after the advent of SDSS, which has permitted many extensive studies of galaxies, the processes involved remain unclear. Hao et al. (2005) estimated that 4−10% of all galaxies in the SDSS harbor an AGN;

⋆ Table 4 is available in electronic form at http://www.aanda.org

Kauffmann et al. (2003) estimated that up to 80% of galaxies more massive than 10^{11} $M_{\odot}$ host a supermassive black hole, either dormant or active. The role of the environment in triggering or inhibiting nuclear activity remains disputed. Kauffmann et al. (2004), analyzing ∼122 000 SDSS spectra, found a decrease in the fraction of powerful AGNs (with high [OIII] luminosity, i.e. dominated by Seyferts) with increasing galaxy environment density, mainly because the most powerful AGNs are hosted by late-type galaxies, which are the least likely to exist in dense environments. Popesso & Biviano (2006) found that the AGN fraction decreases with the increasing velocity dispersion of galaxies in groups and clusters, being higher in dense, low-dispersion groups, in contrast to the findings of Shen et al. (2007) & Miller et al. (2003) who found that the frequency of low activity AGNs does not correlate with environment.

The classification of AGNs based on optical spectra has been traditionally performed using the BPT diagnostic diagram of Baldwin et al. (1981), which adopts the measurement of at least four spectral lines: Hβ, O[III], Hα, and N[II]. The ratio Hα/N[II] (where Hα must be corrected for any underlying stellar absorption, as stressed by Ho et al. 1997) differentiates AGNs from HII region-like nuclei, while the ratio Hβ/O[III] allows us to separate the strong AGNs from the weaker LINERs. More recently Cid Fernandes et al. (2010, 2011) introduced a two-line diagnostic diagram, named WHAN, based on the Hα/N[II] ratio combined with the strength of the Hα line (corrected for underlying stellar absorption) to discriminate both strong and weak AGNs, which are both supposed to be ionized by active black holes, from "fake AGNs", dubbed "retired galaxies", whose ionization mechanism is provided by their old stellar population. As argued by several authors (e.g. Trinchieri & di Serego Alighieri 1991; Binette et al. 1994; Macchetto et al. 1996; Stasińska et al. 2008; Sarzi et al. 2010; Capetti & Baldi 2011), hot evolved stars, such as post-asymptotic giant branch stars and white dwarfs, can produce a substantial diffuse field of ionizing photons: it has been shown that they can produce emission lines with ratios mimicking those of AGNs and – in particular – of LINERs.

An equivalent width (EW) of Hα of at least 3 Å is ultimately required for a nucleus to be considered ionized by a central black hole (Cid Fernandes et al. 2010, 2011). This quantitative threshold of course might be questioned. Among the galaxies in our sample, we might consider for example the elliptical NGC 3862 (CGCG 97-127), which is the second brightest galaxy of A1367 and was classified as an AGN by Véron-Cetty & Véron (2006). It harbors the radio galaxy 3C-264 (Gavazzi et al. 1981) and an optical jet (Crane et al. 1993), leaving little doubt that it contains a central monster. Its optical spectrum (taken either at Loiano or from SDSS) displays a strong NII emission line (of EW 4.81 Å) and a weak Hα EW of 1.51 Å. After adding 1.3 Å to the underlying absorption, the galaxy just misses the Hα > 3 Å threshold, thereby fails to be classified as a LIN but not as a RET according to the criteria of Cid Fernandes et al. (2010, 2011)[1].

The Coma supercluster, on which this paper is focused, is an ideal laboratory for initiating a complete census of AGNs at $z = 0$ because problems related to the incompleteness of SDSS are less severe here than elsewhere. Even its largest sized galaxies have diameters <2−3 arcmin, making the "shredding" problem much less severe than for other nearby environments (e.g. Virgo). The brightest galaxies have been well-studied and even the faintest galaxies belonging to the Coma supercluster have sizes in excess of 10 arcsec, allowing their classification by visual inspection on SDSS plates. Moreover, at the distance of 100 Mpc in the Coma supercluster, the three arcsec fibers adopted by SDSS provide truly "nuclear" spectra. Studying the Coma supercluster using both the integrated and nuclear properties of galaxies at $z = 0$ derived from SDSS data, allows us to compare galaxies properties for a variety of environmental conditions, from the center of two rich clusters to the sparse filamentary regions where the local galaxy density is ∼100 times lower, without the biases caused by studying galaxies at different distances. It provides a complementary view to the many statistical analyses that have been made using SDSS data (e.g. Kauffmann et al. 2004). Combined with studies of galaxy evolution at higher redshift it will shed light on the mechanisms and processes that contribute to the evolution of galaxies in the cosmological context.

Owing to the two-line WHAN diagnostics, the red-channel spectra taken at Loiano can contribute significantly to the census of AGNs by filling the residual incompleteness of the SDSS spectral database for luminous galaxies caused by shredding and fiber conflict (Blanton et al. 2005a,b,c).

The layout of this paper is as follows. In Sect. 3, we illustrate the observations taken at the Loiano observatory and the data reduction procedures. The nuclear spectra are given and classified in Sect. 4. The census of AGNs of the various types in the Coma supercluster is carried out in Sect. 5. Our results are compared with Mahajan et al. (2010) and discussed in Sect. 6. The standard cosmology is assumed, with $H_0 = 73$ km s^{-1} Mpc^{-1}.

2. The sample

This paper is based on two samples:

i) a miscellaneous set of 283 relatively bright galaxies, not complete by any means, for which we took long-slit, red-channel nuclear spectra of $R \sim 1000$, with the Loiano telescope. We refer to this as the "LOI sample" hereafter;
ii) a complete set of 5027 galaxies (hereafter the "COMA sample") selected in the region $11.5^{\rm h} < {\rm RA} < 13.5^{\rm h}; +18° < {\rm Dec} < 32°$ (see GoldMine, Gavazzi et al. 2003) that traditionally describes the Coma supercluster and was extensively studied by Gavazzi et al. (2010), combined with an extended region defined by $10^{\rm h} < {\rm RA} < 16^{\rm h}$ and $+24° < {\rm Dec} < 28°$ (see Fig. 1). The second area is suitable for filling an LST interval corresponding to the duration of an observing night in spring and has also been covered with HI observations by ALFALFA (Giovanelli et al. 2005), whose HI selected targets will shortly be publicly available.

Following the method of Gavazzi et al. (2010), we searched in this area of the sky ($11.5^{\rm h} < {\rm RA} < 13.5^{\rm h}; +18° < {\rm Dec} < 32°$ combined with $10^{\rm h} < {\rm RA} < 16^{\rm h}; +24° < {\rm Dec} < 28°$) the SDSS DR7 spectroscopic database (Abazajian et al. 2009) for all galaxies with $r \leq 17.77$ in the redshift interval $3900 < cz < 9500$ km s^{-1}. We obtained 4790 targets. For each, we extracted the coordinates, u, g, r, i, z Petrosian magnitudes (AB system), and spectroscopic information, including the principal line intensities and the redshift. The morphological classification of all galaxies was performed by individual visual inspection of SDSS color images.

To fill-in the incompleteness of SDSS for luminous galaxies due to shredding and fiber conflict (Blanton et al. 2005a,b,c), we added 133 CGCG (Zwicky et al. 1961−1968) galaxies with known redshifts from NED that were not included in the SDSS spectral database (see Fig. 2). For these objects, we also

[1] Similar examples (see Sect. 4) convinced us to lower the threshold for LIN from 3 Å to 1.5 Å in the present analysis.

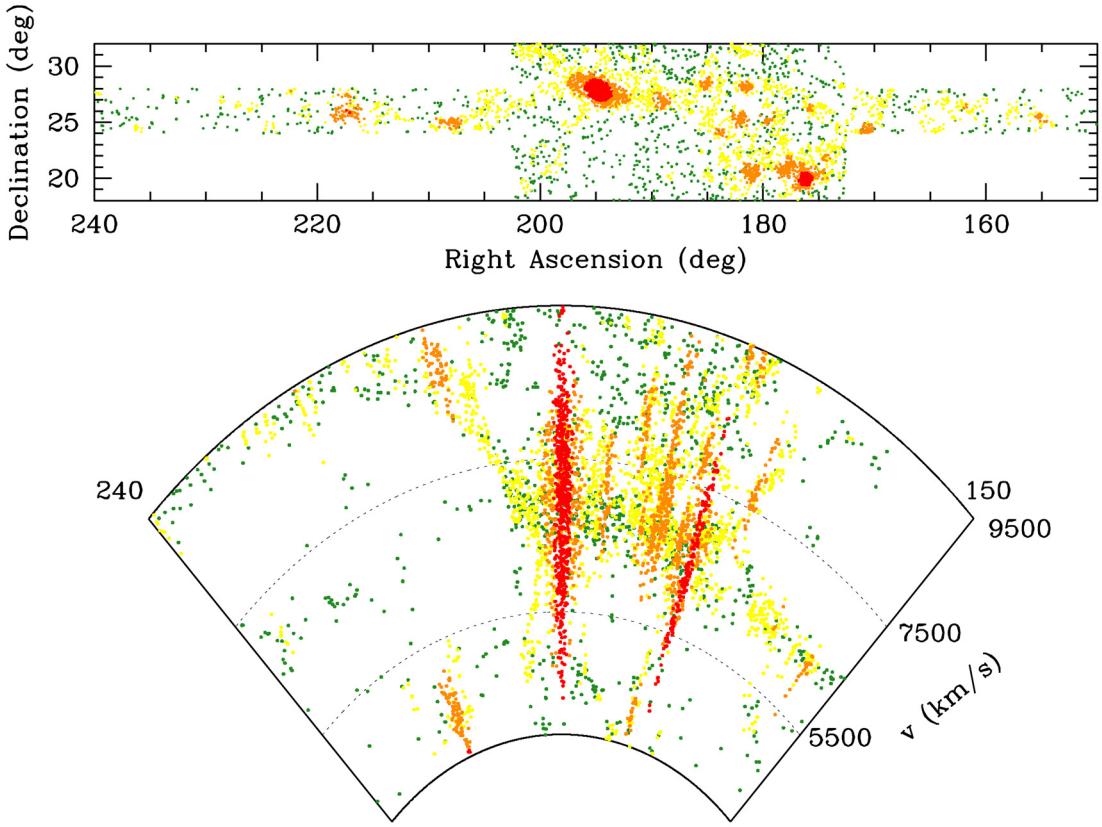

Fig. 1. (*Top panel*) The Coma supercluster region studied in this work in celestial coordinates and as a wedge-diagram. (*Bottom panel*) Symbols are color coded according to the density parameter (see Sect. 5): UL: $\delta_{1,1000} \leq 0$ are green; L: $0 < \delta_{1,1000} \leq 4$ are yellow; H: $4 < \delta_{1,1000} \leq 20$ are orange; UH: $\delta_{1,1000} > 20$ are red.

measured the u, g, r, i, z Petrosian magnitudes using the SDSS DR7 navigation tool, which provides accurate magnitudes.

Additional galaxies that could not be found in the SDSS spectroscopic catalog were searched for using NED. For these targets, we again evaluated the u, g, r, i, z magnitudes using the SDSS navigator tool and among them we selected 76 objects meeting the condition $r \leq 17.77$, which matches the selection criterion of the SDSS spectral catalog (Strauss et al. 2002). We repeated a similar search in the ALFALFA database (Haynes, private communication) for the region $10^h < RA < 16^h$ and $+24° < Dec < 28°$, and found 28 additional HI-selected systems with $r \leq 17.77$, not included in the SDSS spectral database. In total, our sample consists of 5027 galaxies: 4790 from SDSS and 237 from other sources.

The 4785 out of 4790 galaxies selected from SDSS have a spectrum available from the SDSS database (five remaining objects have partly corrupted spectra); another 130 were observed at Loiano, taken from sample i), and the remaining 112 do not yet have available spectra. In total, the "COMA sample" reaches a spectral completeness of 98%.

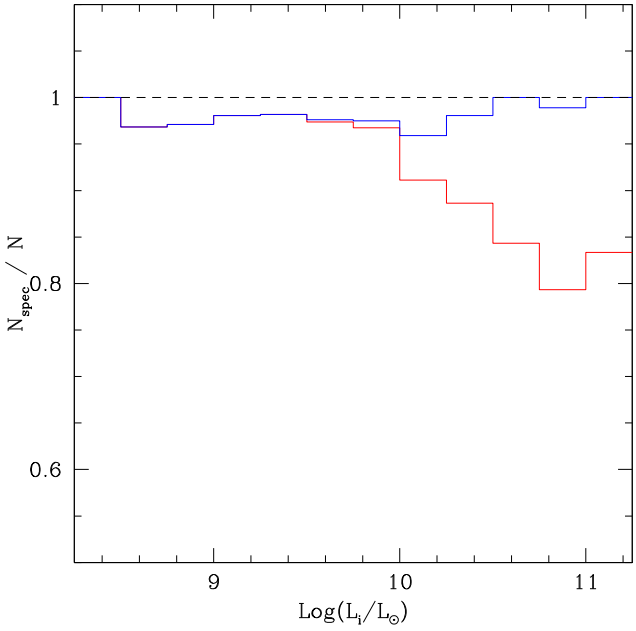

Fig. 2. The completeness of the "COMA sample", consisting of galaxies taken from SDSS, targets taken from CGCG, NED, and ALFALFA, and objects with spectra taken at Loiano (blue), is 98% (only 112 galaxies remaining without nuclear spectra). Galaxies selected from the SDSS alone (red), e.g. used by Mahajan et al. (2010) are incomplete by ~20% in the highest luminosity bins, where most AGNs are expected.

3. Observations and data reduction

Optical spectra of the nuclei of 283 galaxies in sample i) were obtained during 14 runs from 2005 to 2011 (see Table 1) using the Bologna Faint Object Spectrograph and Camera (BFOSC) attached to the 152 cm F/8 *Cassini* Telescope located in Loiano, belonging to the Observatory of Bologna. These consist of long-slit spectra taken through a two-arcsec slit, combined with

Table 1. Log of the observations at Loiano.

Year	Feb.	Mar.	N_{spec}
2005	9, 10, 11	9, 11, 12	45
2006	26	23	24
2007	13, 15, 16	17, 18	29
2008	5	3	10
2009	18, 19, 21	26, 27	54
2010	8	–	10
2011	7, 8, 9, 10	6, 7, 8	133

Notes. Two new-moon periods of four nights each were allocated to the present project per year. We list information for the useful nights. The total number of spectra (305) includes 22 of objects that were repeatedly observed during several runs. In these cases, Table 2 describes the combined spectra.

an intermediate-resolution grism ($R \sim 1000$) covering the 6100–8200 Å portion of the red-channel and containing Hα, [NII], and [SII] spectral lines. BFOSC is equipped with a EEV LN/1300-EB/1 CCD detector of 1300 × 1340 pixels, reaching 90% QE near 5500 Å. For the spatial scale of 0.58 arcsec/pixel, the useful field is of 12.6 × 13 square arcmin. The grism dispersion of 8.8 nm/mm results in spectra with 1.6 Å/pix. Exposures of 3–5 min were repeated typically three times (to help remove the cosmic ray hits), up to six times. The slit was generally set in the E-W direction, except when aligned along the galaxy major axis, or along the direction connecting two nearby objects taken simultaneously in the slit. The wavelength calibration was secured by means of frequent exposures of a He-Ar hollow-cathode lamp. The flux calibration and the spectrograph response were obtained by daily exposures of the star Feige-34. The typical seeing conditions at Loiano ranged from 1.5 to 2.5 arcsec.

The reduction of the spectra was based on the IRAF STSDAS[2] reduction packages. The wavelength calibration was performed on the lamp exposures using *identify-reidentify-fitcoo* and transferred to the scientific exposures using *transform*. After checking the wavelength calibration using the principal sky lines, these were removed using *background*. One-dimensional (1d) spectra of the nuclei were extracted from the two-dimensional (2d) images using *apsum* in apertures of 5.8 arcsec. After flux calibration, the 1d spectra were normalized to the intensity of the continuum under Hα, transformed to rest-frame velocity, and measured with *splot* to obtain the EW of the Hα and λ 6584 [NII] lines.

4. Spectral classification

The classification of the nuclear activity based on optical spectra was performed according to identical rules for sample i) LOI and ii) COMA (except for Seyfert galaxies; see below in this section). The classification rule is based on the WHAN diagram introduced by Cid Fernandes et al. (2010, 2011), which is based on the strength of the Hα line corrected for underlying stellar absorption (Ho et al. 1997) and the ratio of [NII] to Hα_{corr} (EW) to discriminate between different levels of nuclear activity. As for the underlying absorption at Hα, Decarli et al. (2007) adopted an average correction of 1.7 Å. Owing to the limitations of the SDSS spectral database, this quantity is here determined again to greater accuracy using 881 SDSS spectra of passive galaxies in the Coma supercluster (see Table 3). The mean underlying stellar absorption at Hα present in all passive galaxy spectra amounts to 1.3 Å, irrespective of luminosity, below or above Log($L_i/L_\odot$) = 10[3]. Thus we adopt 1.3 Å for the underlying continuum absorption at Hα, i.e. Hα_{corr} = Hα − 1.3 Å.

Figure 3 shows the WHAN diagram with the adopted spectral classification thresholds. The vertical line shows the separation between HII region-like nuclei and AGNs. This threshold is set at log(EW[NII]/EWHα_{corr}) = −0.30 in agreement with Capetti & Baldi (2011), as a compromise between the value of −0.22 adopted by Baldwin et al. (1981) and Decarli et al. (2007), and the value of –0.40 adopted by Cid Fernandes et al. (2010, 2011)[4].

In Fig. 3, several EWHα_{corr} thresholds are indicated. These are used to discriminate between the various levels of nuclear activity, as recommended by Cid Fernandes et al. (2010, 2011) with one difference: the separation between both HII regions and weak AGNs (LIN) from "fake ones" (RET) is set to |EWHα_{corr}| = 1.5 Å instead of 3 Å[5]. Summarizing, we define six independent classes of nuclear activity:

- "HII region-like" nuclei are characterized by intense star-formation activity: their spectra display both Hα and [NII] in emission, with |EWHα_{corr}| > 1.5 Å and the ratio log(EW[NII]/EWHα_{corr}) < −0.3;
- strong AGN (sAGN) contain a powerful active nucleus (possibly triggered by a supermassive black hole): their spectra have |EWHα_{corr}| > 6 Å and log(EW[NII]/EWHα_{corr}) > −0.3;
- weak AGNs (LIN) show the signature of a less active nucleus than sAGN: their spectra have 1.5 < |EWHα_{corr}| < 6 Å and log(EW[NII]/EWHα_{corr}) > −0.3;
- fake AGNs (RET) are thought to be "retired nuclei" whose ionization mechanism is provided by their old stellar

[2] IRAF is the Image Analysis and Reduction Facility made available to the astronomical community by the National Optical Astronomy Observatories, which are operated by AURA, Inc., under contract with the US National Science Foundation. STSDAS is distributed by the Space Telescope Science Institute, which is operated by the Association of Universities for Research in Astronomy (AURA), Inc., under NASA contract NAS 5–26555.

[3] For star-forming galaxies, the direct determination of absorption is hampered by the presence of Hα and [NII] in emission. However, for bright spirals (Log($L_i/L_\odot$) > 10, often dominated by bulges) the presence of underlying absorption at Hα is sometimes detected (although difficult to quantify) in the SDSS spectra. In contrast, for faint late-types (Log($L_i/L_\odot$) ≤ 10) the absorption component at Hα is generally not detected, being overtaken by the emission component, which amounts on average to 30 Å (and exceeds 5 Å for 93% of them), making the 1.3 Å correction negligible.

[4] With this choice, two galaxies (NGC 3773 and CGCG136-042) classified as HII regions in NED are inconsistently classified as LINER by ourselves because they have −0.3 < log(EW[NII]/EWHα_{corr}) < −0.22, but another two (NGC 2537 and CGCG 71068), classified as HII regions by both NED and us, would have been inconsistently classified as LINERS by Cid Fernandes et al. (2010, 2011).

[5] This choice is adopted because well-established LINERS e.g. VCC1110 (Véron-Cetty & Véron 2006), VCC2070 (Panessa & Bassani 2002), NGC 2841 (Véron-Cetty & Véron 2006), NGC 6166 (containing the radio galaxy 3C-338, Gavazzi & Perola 1980), CGCG 97-127 (Véron-Cetty & Véron 2006; containing the radio galaxy 3C-264, Gavazzi et al. 1981; with optical jet Crane et al. 1993), which would otherwise have been classified as RET by Cid Fernandes et al. (2010, 2011), are consistently classed among LIN. Even after weakening the criterion for LIN to |EWHα_{corr}| > 1.5 Å, some inconsistencies remain between our classification and NED: NGC 2685 (classified as Sey2 by Véron-Cetty & Véron 2006) and VCC1615 (classified as LIN by Véron-Cetty & Véron 2006) are classified as RET in this work.

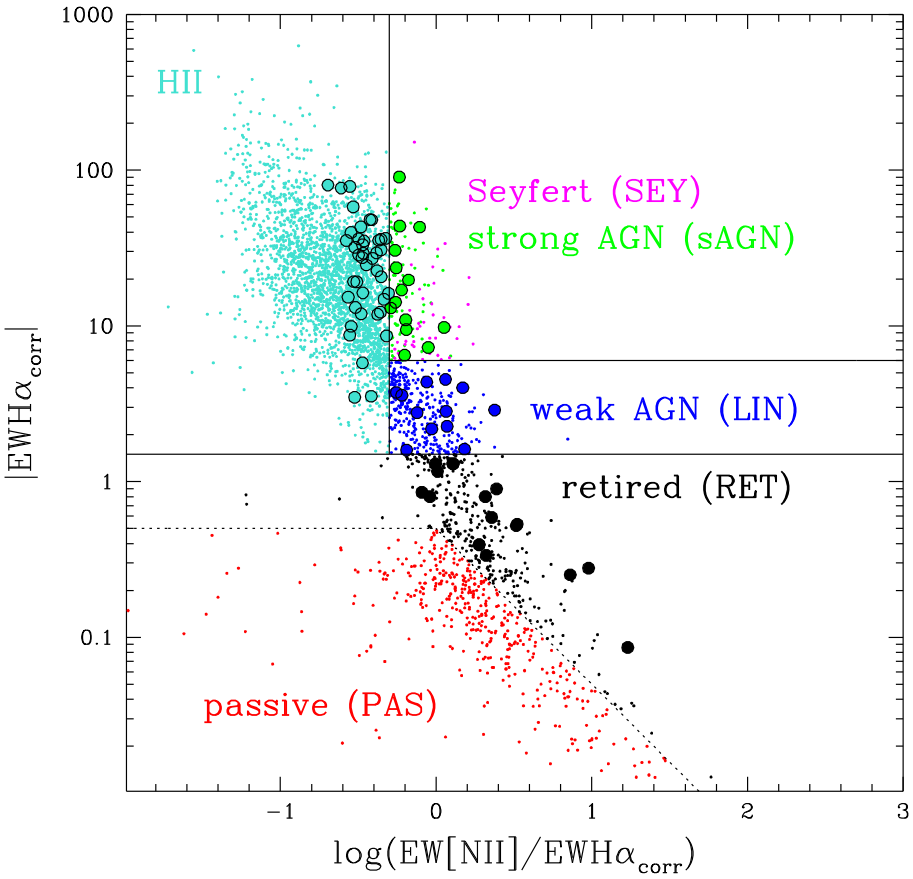

Fig. 3. The WHAN diagnostic diagram. The equivalent width of Hα is corrected by 1.3 Å for underlying absorption. Small symbols refer to the COMA sample, large symbols to the LOI sample. Seyfert1 galaxies, identified visually in the Loiano spectra, are given as triangles.

Table 2. Line measurements performed on stacked Loiano spectra of N objects in six spectral classes in the "LOI sample".

Class	N	EWHα	EW[NII2]
HII	106	–25.4	–9
SY1	10	–30	-24
sAGN	41	–13.6	–9.1
LIN	42	–1.7	–3.0
RET	12	1.0	–1.1
PAS	42	1.6	0.0

Notes. Negative = emission.

Table 3. Line statistics in the "COMA sample" containing N objects in each spectral class.

Class	N	EWHα	EW[NII2]
HII	2721	–28.7	–5.9
SEY	48	–13.4	–12.6
sAGN	103	–22.8	–14.8
LIN	331	–1.7	–2.5
RET	436	1.0	–1.0
PAS	881	1.3	–0.2

Notes. Negative = emission.

population in a way that can mimic the processes of AGNs and – in particular – of LINERs: their spectra have either Hα in moderate absorption ($0.5 < |\mathrm{EWH}\alpha_{\mathrm{corr}}| < 1.5$ Å) or both Hα in absorption ($|\mathrm{EWH}\alpha_{\mathrm{corr}}| < 0.5$ Å) and [NII] in emission ($|\mathrm{EW[NII]}| > 0.5$ Å);

– passive nuclei (PAS) are typically red, contain exclusively old stars, with no star formation activity: their spectra show both Hα and [NII] in absorption ($|\mathrm{EWH}\alpha_{\mathrm{corr}}| < 0.5$ Å and $|\mathrm{EW[NII]}| < 0.5$ Å).

The classification of Seyfert galaxies follows different rules for the "LOI sample" and SDSS spectra. For SDSS spectra, we use EW[OIII]/EWH$\beta > 3$ to identify Seyfert (SEY) among sAGN. In the "LOI sample", the absence of blue-channel spectra prevents us from using the BPT diagnostic diagram, hence Seyfert1 galaxies (SY1, represented with pink triangles in Fig. 3) are classified by visual inspection of individual spectra for the presence of broad permitted lines. Tables 2 and 3 summarize the classification of spectra, respectively, in the "LOI" and "COMA" samples.

Template spectra of the six spectral classes, obtained by stacking N spectra taken at Loiano, are given in Fig. 4 (LOI top panel). The 4785 FITS spectra available from SDSS were downloaded, shifted to their rest-frame using *IRAFdopcor*, and normalized to the flux intensity near Hα. The rms of their continuum were measured between 6230 Å and 6490 Å (avoiding bright galaxy spectral lines and sky residuals), providing an estimate of the signal-to-noise ratio (S/N). Spectra with $S/N > 10$ were stacked in each spectral class and are shown in Fig. 4 (COMA bottom panel).

The parameters of the 283 individual spectra for the "LOI sample" are listed in Table 4 as follows: Col. 1: Galaxy name; Cols. 2 and 3: J2000 celestial coordinates; Col. 4: redshift from NED; Cols. 5 and 6: measured EW of Hα and λ 6584 [NII] lines from the present work (negative values represent emission); Col. 7: the nuclear activity classification in six bins; Col. 8: other spectra available from either SDSS or NED (*SDSS-corr* means that the SDSS spectrum is partly corrupted); Col. 9: independent classification of the nuclear activity from NED.

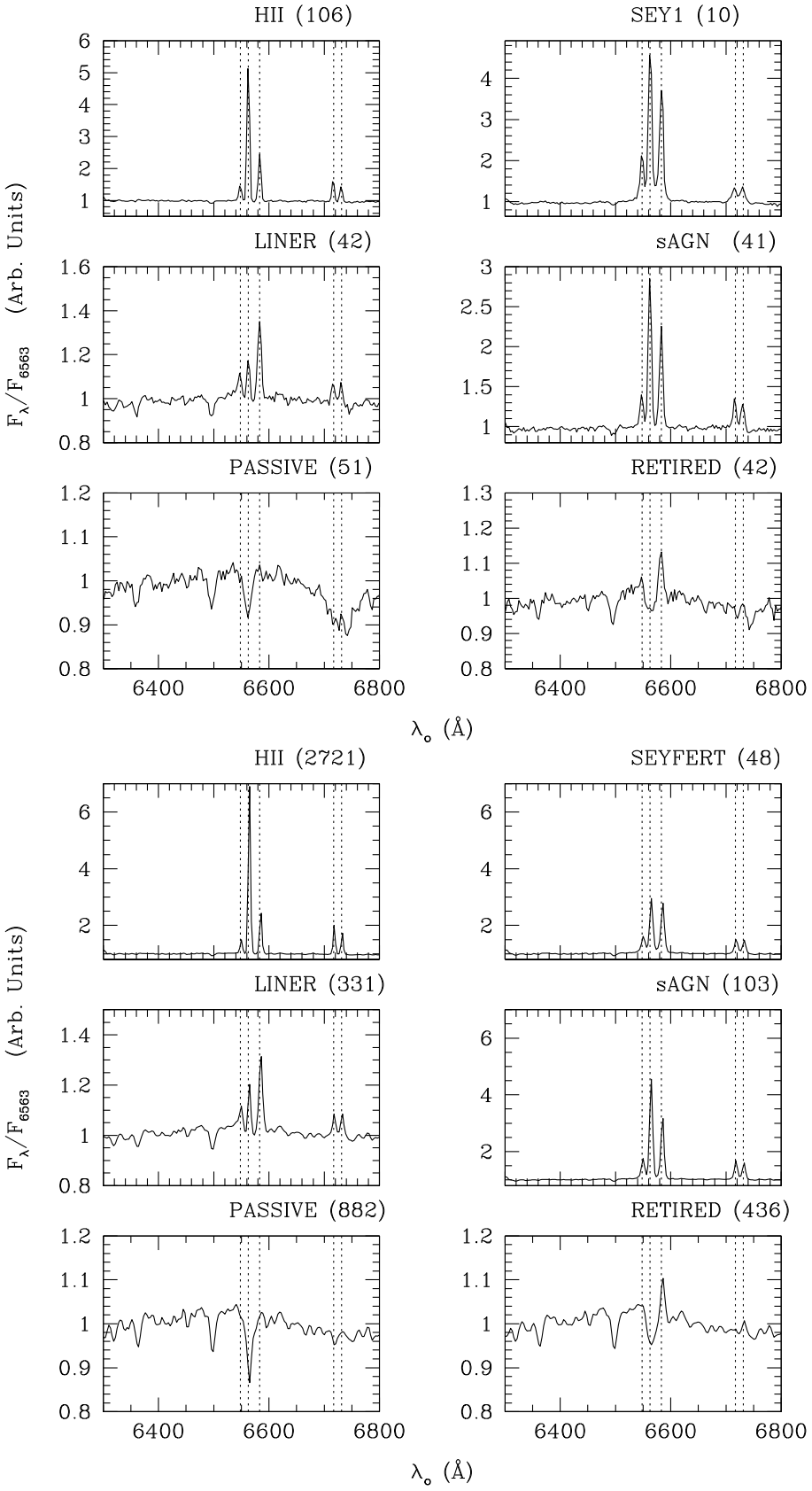

Fig. 4. Template spectra obtained by stacking individual normalized rest-frame spectra (whose number is given in parenthesis) in six bins of nuclear classification. The vertical dashed lines mark the position of [NII] λ 6548, Hα λ 6563, [NII] λ 6584, and the [SII] doublet λ 6718 and λ 6733. "LOI sample (*top panel*); "COMA sample" (*bottom panel*).

As anticipated in Sect. 2, the 283 "LOI sample" galaxies do not form a complete sample in any sense. Among them, 41 belong to the Virgo cluster, which are not considered further here. Not all of the 177 galaxies belonging to the Coma supercluster have new spectroscopic measurements: several have also a nuclear spectrum (acquired using three arcsec fibers) from the DR7 of SDSS and many others have nuclear spectra available from NED. Nevertheless, there are 130 Coma galaxies in the "LOI sample" (see Table 4) that do not have a spectrum in SDSS, hence these data contribute toward the completion of the

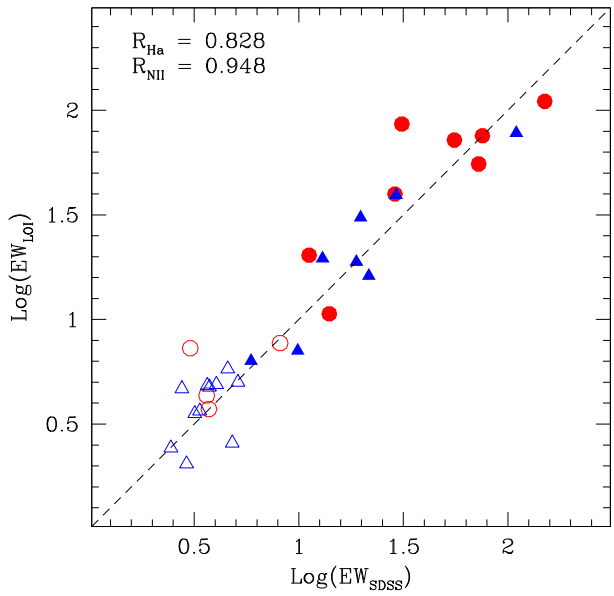

Fig. 5. The equivalent width of Hα (red dots) and λ 6584 [NII] (blue triangles) for 15 galaxies in the Coma supercluster that were measured both at Loiano and by SDSS. The correlation coefficients are given. The dashed line gives the 1:1 relation. Empty symbols refer to galaxies with luminosity Log($L_i/L_\odot$) > 10.5.

"COMA sample" (see Sect. 5). For 15 Coma galaxies taken at Loiano before the DR7 of SDSS was issued, Fig. 5 displays the two independent measurements of the EW of Hα and λ 6584 [NII], which do not appear to be affected by systematic errors[6].

5. AGNs in the Coma supercluster

The data obtained in the previous section are used to help perform a census of AGNs in the Coma supercluster region.

Following an identical procedure to Gavazzi et al. (2010), the local number density ρ around each galaxy was computed within a cylinder of 1 h^{-1} Mpc radius and 1000 km s^{-1} half-length. We divide the sample into four overdensity bins, chosen in order to highlight physically different environments of increasing level of aggregation: the Ultra-Low density bin (UL: $\delta_{1,1000} \leq 0$) describing the underlying cosmic web; the Low density bin (L: $0 < \delta_{1,1000} \leq 4$) comprising the filaments in the Great Wall and the loose groups; the High density bin (H: $4 < \delta_{1,1000} \leq 20$) including the cluster outskirts and the significant groups; and the Ultra-High density bin (UH: $\delta_{1,1000} > 20$) corresponding to the cores of rich clusters.

Figure 1 shows the celestial distribution and the wedge diagram for the 5027 galaxies in the "COMA sample", coded according to the four density bins.

Figure 6 (top panel) gives the $g-i$ color vs. i-band luminosity diagram for the studied galaxies, highlighting the distribution of galaxies without an SDSS spectrum and that the spectra taken at Loiano (filled dots) were obtained deliberately for bright objects with Log($L_i/L_\odot$) > 10, where the missing spectra from SDSS are more abundant and AGNs are more frequently found (Decarli et al. 2007). Out of the 112 galaxies remaining with no spectra (empty circles), only 30 are brighter than Log($L_i/L_\odot$) = 10. Among them, we expect to miss approximately 10 AGNs, given the luminosity distribution of AGNs discussed below.

Before discussing the various color diagrams, we emphasize that the contribution of AGNs to the total i luminosity is negligible, as the light measured in nuclear apertures of three arcsec diameter for the most luminous of all AGNs, i.e. the Seyferts, represents between 5% and 15% of the total light.

Figure 6 (middle panel) shows the position of HII, SEY, and sAGN in the color-magnitude diagram, clearly showing that AGNs of high activity belong to the high luminosity tail of the sequence composed of star-forming galaxies (their slope is 0.34, and the dispersion is 0.20). Figure 6 (bottom panel) illustrates the position of PAS, RET, and LIN, showing that AGNs of low activity, including fake-AGNs, belong to the high luminosity part of the "red sequence" (their slope is 0.17, and the dispersion is 0.10). LIN follow a relation with a slightly higher slope (0.20) and dispersion (0.14) than RET and PAS alone (slope = 0.16, and dispersion = 0.09), suggesting that they might belong to a transition class between early- and late-type galaxies. From Fig. 6 (middle and bottom panels), we can see that many luminous objects, mostly AGNs, have redder colors than red-sequence galaxies of similar luminosity and in particular of PAS. These galaxies are strongly affected by extinction from dust lanes.

We have measured the average $g-i$ for the whole galaxy in the three classes of AGNs of decreasing activity (SEY, sAGN, LIN) and among RET. The resulting mean color for the four classes is $\langle g-i \rangle \simeq 1.15 \pm 0.15$ mag, consistent with the average color of galaxies in the red sequence and of PAS galaxies. This value is not found to depend on the local galaxy density. The only class with $\langle g-i \rangle \simeq 0.72$, which is significantly bluer than all other classes, is the one of HII-like nuclei. Since $g-i$ color can be assumed as a proxy of the star formation in galaxies, this result seems to support the evolutionary scenario where the feedback from AGNs produces a significant quenching of the star formation in their host galaxies (e.g. Schawinski et al. 2009). However, our finding neither proves nor disproves this hypothesis because the same mean color might be found for PAS galaxies, which do not necessarily originate from a previous AGN phase, but simply from the fading of a nuclear starburst phase.

The morphology distribution of AGNs, including RET, is given separately in Fig. 7 (top panel). It appears that sAGN and SEY are mostly (40%) associated with giant spiral galaxies (Sa-Sb) (and another 29% to S0a). LIN and RET are 78% associated with early-type galaxies (E-S0a).

Among non-AGNs (Fig. 7 bottom panel), PAS are 94% associated with E-S0, while HII regions are 87% associated with late-type galaxies (Sa-BCD).

The differential luminosity distribution of all AGNs (SEY+sAGN+LIN) (with and without RET) is given in Fig. 8. For all galaxies, the luminosity distribution follows a Schechter function (whose parameters can be found in Gavazzi et al. (2010). For the AGNs, the distribution is instead "Gaussian", with a peak near Log($L_i/L_\odot$) = 10.2. Below this luminosity (Log($L_i/L_\odot$) ≤ 10.2), the fraction of Active Nuclei is 11% with RET and 6% without. For Log($L_i/L_\odot$) > 10.2, it becomes 60% with and 32% without RET. RET alone represent a similar fraction of all bona-fide AGNs at any luminosity.

When the frequency of galaxies in the various spectral classification bins (normalized to the total number of surveyed

[6] The extraction of the Loiano spectra was carried out in apertures whose area (11.6 arcsec^2) is almost twice as large as that of the SDSS fibers (7.1 arcsec^2). This was done on purpose to compensate for the Loiano spectra being taken for the brightest galaxies, which are a factor of two, on average, larger than those taken by SDSS. Figure 5 shows no systematic effects for bright and faint objects.

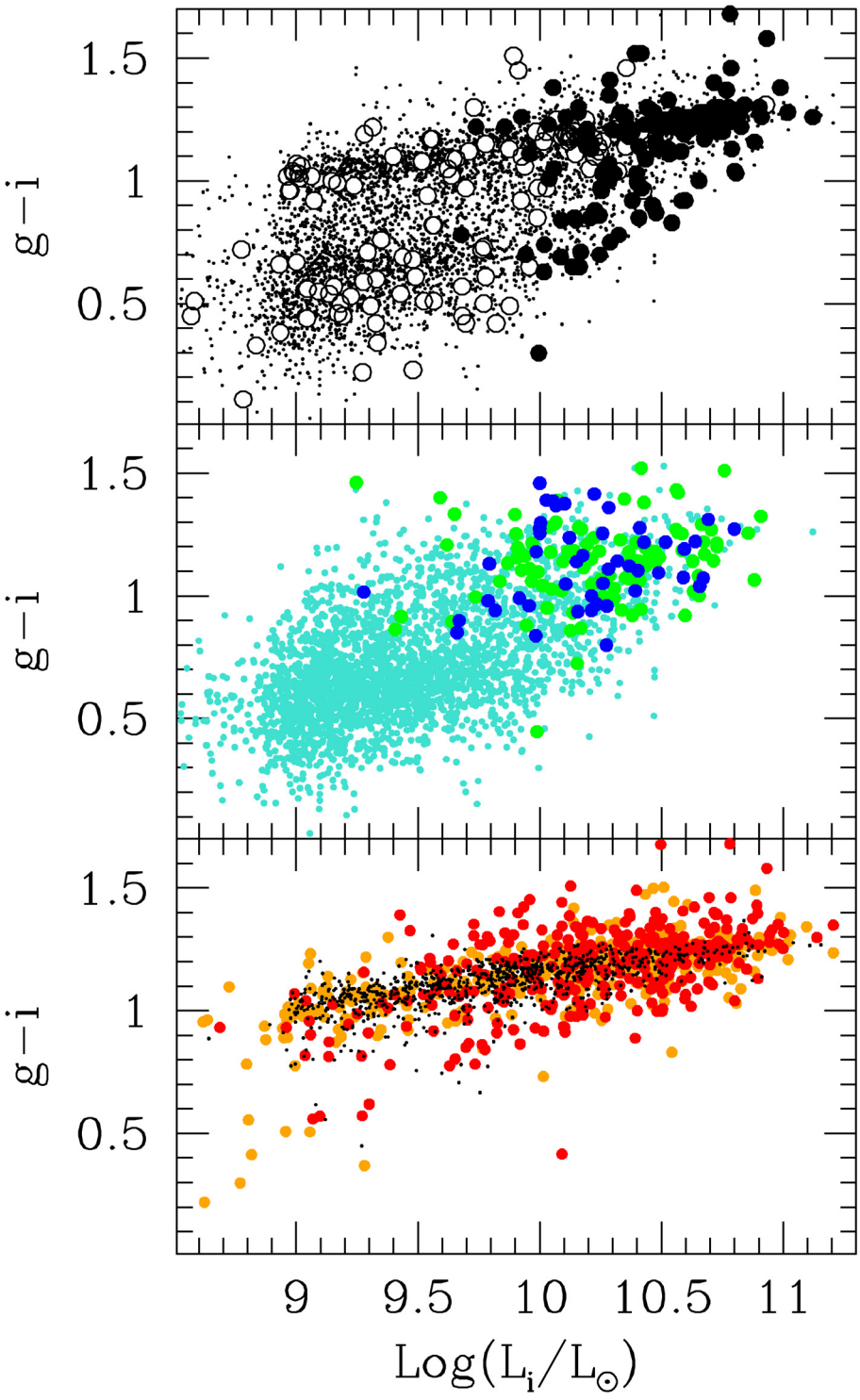

Fig. 6. The color ($g - i$) vs. i-luminosity diagram of galaxies studied in this work. *Top panel*: small black dots represent the 4900 galaxies from SDSS; large filled symbols mark the 130 galaxies for which a nuclear spectrum was taken at Loiano, and large open symbols mark the 112 galaxies yet without spectra. *Middle panel*: HII regions (turquoise), SEY (blue), and sAGN (green) form the blue sequence. *Bottom panel*: LIN (red), RET (orange), and PAS (black) form the red sequence.

galaxies) is plotted in bins of local galaxy density, it appears (see Fig. 9) that:

- among AGNs, the percentage of SEY-sAGN-LIN does not change significantly from UL to H density but decreases by a factor of two in the densest UH environment (notice that LIN are as frequent in the lowest and highest density bins);
- among non-AGNs, the fraction of HII-like nuclei decreases gradually with increasing density, overall by a factor of four. RET and PAS increase by a factor of two and four respectively. A similar result was obtained by Miller et al. (2003).

The second result need not imply that the local environment has a direct influence on the nuclear activity of galaxies, but partly reflects the influence of the environment on the "extended galaxy" that harbors some nuclear activity, also called "morphology segregation" (Dressler 1980). To distinguish the two effects, it is recommended that we normalize the number of objects in the various classes of nuclear activity not to the total number of surveyed galaxies (irrespective of the morphological type) but the number of galaxies of certain type classes, as in Fig. 10. Guided by the distribution of AGNs with respect to the Hubble classification (Fig. 7), it is apparent that (among AGNs) SEY and sAGN are more frequent in S0a-Sb, while LIN are frequent in E-Sbs. Among non-AGNs, HII are frequent in all late-type galaxies (including S0a and BCD), RET are found among early-type galaxies (i.e. dE, dS0, E, S0+S0a) and PAS in dE, dS0, E,

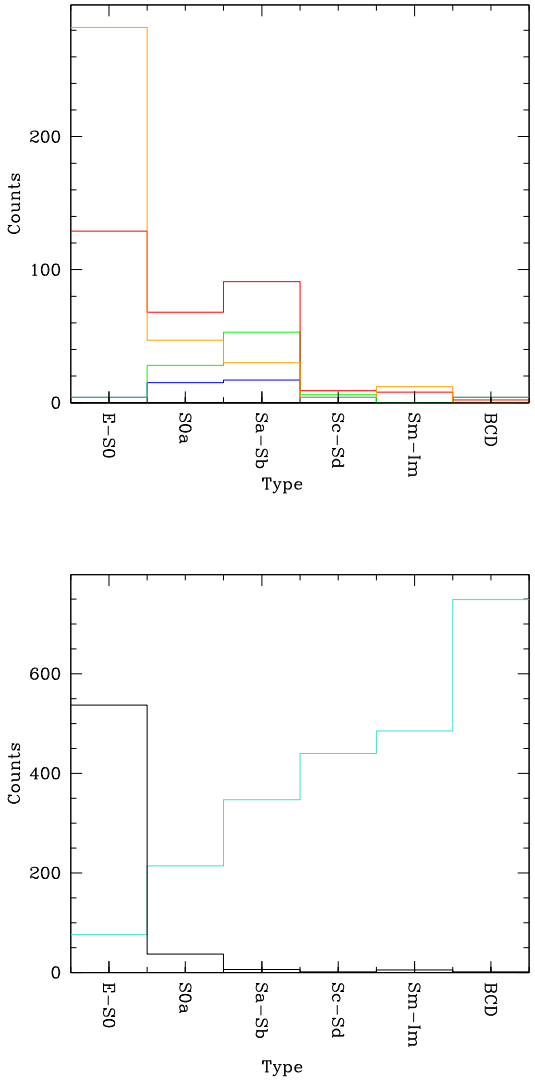

Fig. 7. The morphology distribution of: (*top panel*) SEY (Blue), LIN (red), sAGN (green), RET (orange); (*bottom panel*) HII (turquoise), PAS (black).

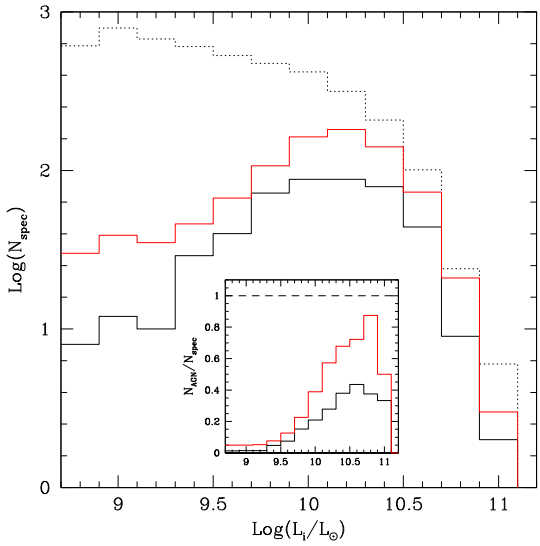

Fig. 8. The luminosity distribution of AGNs with (red) and without (solid black) RET and of all galaxies (dotted). The inset shows the ratio of AGNs to all galaxies with (red) and without (solid black) RET.

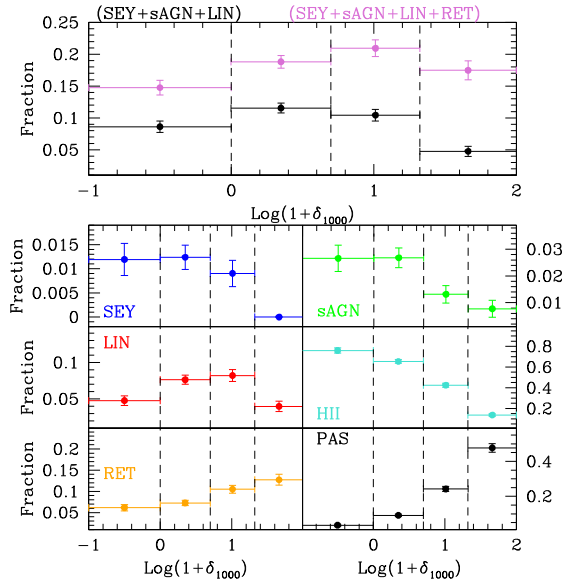

Fig. 9. The frequency distribution of SEY (*top left*); sAGN (*top right*); LIN (*middle left*), HII (*middle right*); RET (*bottom left*); PAS (*bottom right*) and all AGNs (*top*) with RET (pink) and without RET (black) in 4 bins of local galaxy density.

S0. Figure 10 allows us to study the nuclear activity of galaxies irrespective of "morphology segregation". In other words, Fig. 9 includes the effects of the environment on the galaxy as a whole (morphology) and on the nuclear region, while Fig. 10 emphasizes the effects of the environment on the nuclear region alone.

In conclusion (see Fig. 10):

- the fraction of AGNs associated with both late- and early-type giant galaxies is lower at most by a factor of two in the densest galaxy environment;
- the fraction of star-forming (HII) galaxies is lower by a factor of at most two in the densest galaxy environment;
- the fraction of ex-star-forming (RET) galaxies decreases gradually by a factor of two with increasing density from the lowest to the highest density bin;
- the fraction of passive (PAS) galaxies increases gradually by a factor of two with increasing density from the lowest to the highest density bin;
- all signs of nuclear activity, either associated with a central black hole or with star formation, are significantly lower in the cores of the rich clusters than lower density environments.

6. Discussion and conclusion

A dependence of AGN activity on local galaxy density similar to the one found in this work was proposed by Mahajan et al. (2010), who analyzed almost exactly the same sky volume. This apparent agreement is however the consequence of a manifold blunder in their analysis. First of all, the galaxy sample in the Coma supercluster used by them suffers from 20% incompleteness at high luminosity (see Sect. 2) owing to the incompleteness

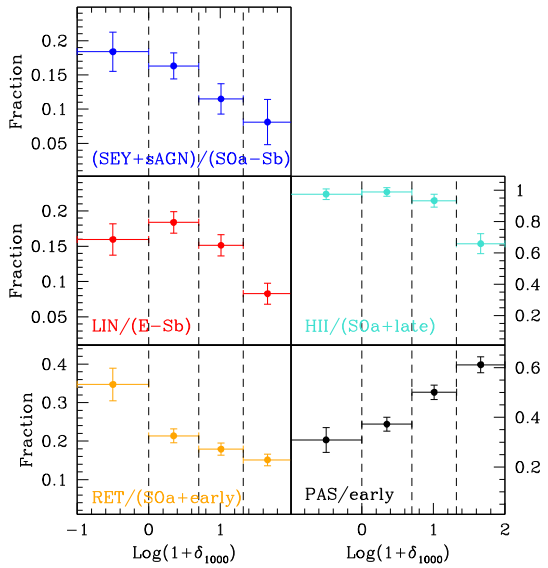

Fig. 10. The frequency distribution of the ratio of SEY+sAGN to giant spirals (SOa-Sb); of LIN to giant galaxies (E-Sb); of RET to early-type galaxies (dE-S0a); of HII to SOa+late-type galaxies; and of PAS to early-type (dE-S0) galaxies in four bins of local galaxy density.

of the SDSS spectral database, which is entirely disregarded in the Mahajan et al. (2010) analysis.

Secondly the Hα spectral line measurements from the SDSS database have not been corrected for underlying stellar absorption. Thirdly the fraction of AGNs is computed by Mahajan et al. (2010) by normalizing to the total number of galaxies, irrespective of their morphology, Owing to the first omission and the adoption of the BPT diagnostic, Mahajan et al. (2010) failed to classify as AGNs an enormous number of objects with [NII] in emission and Hα in weak absorption, particularly ones present in the core of rich clusters, that would increase the frequency of AGNs in the densest environments. At the same time, they overestimated the number of AGNs among galaxies with [NII] and Hα in emission (that become HII like nuclei when corrected). These are predominantly found in the field. If Mahajan et al. (2010) had adopted the correct procedure in producing their BPT diagram, they would have concluded that the fraction of AGNs would increase, not decrease, with galaxy density. The reason why AGNs are missing in clusters is that most galaxies that are bona-fide AGNs according to the BPT diagnostic diagram become fake-AGNs (RET) according to the WHAN diagnostic diagram, making the whole issue of the influence of the environment on the formation of AGNs very slippery.

Using the AGN classification scheme of Kauffmann et al. (2003) based on their revised BPT diagram, Kauffmann et al. (2004) analyzed the properties of powerful AGNs among ~122 000 galaxies with $14.5 < r < 17.77$ and median redshift $z \sim 0.1$, from the SDSS DR1. The subtraction of the underlying stellar continuum was performed by fitting the emission-line-free regions of the spectrum with a model galaxy spectrum. They concluded that powerful AGNs occur predominantly in massive galaxies with $>10^{10}$ $M_{\odot}$, another manifestation of "downsizing" (Cowie et al. 1996; Gavazzi et al. 1996; Fontanot et al. 2009). Powerful AGNs are found among late-type, blue, star-forming galaxies. The decrease in their frequency with increasing galaxy density is mostly due to the decrease in the frequency of galaxies that are able to host AGNs (morphology segregation), but – to a lesser extent – is due to a genuine extra decrease in AGN frequency in high density environments. Von der Linden et al. (2010) argued that galaxies in dense environments are less likely to host a powerful optical AGN or a star-forming nuclear region. The frequency of optical AGNs in early-type galaxies declines in high density environments (by approximately a factor of two between the field and the center of clusters). They interpreted this finding by arguing that AGNs are fueled by mass loss from evolved stars. The mean age of the red galaxies increases towards the cluster center and provides less fuel for the central black hole.

Our analysis, which adopts the criteria of Cid Fernandes et al. (2010, 2011) for the classification of nuclei, is in full agreement with both Kauffmann et al. (2004) and Von der Linden et al. (2010). We conclude that, even after eliminating the effects of morphology segregation (by counting the frequency of nuclear activity in the proper bins of Hubble type), there is a residual decline in the frequency of nuclear activity (either triggered by black holes or sustained by the star formation) with increasing galaxy density (see Fig. 10). At any luminosity, this decline is quantified in a factor of ~2 per interval of density contrast of approximately 20, going from the less dense filaments that form the local cosmic web to the densest cores of rich clusters. Whichever mechanism is responsible for the suppression of over star formation in galaxies, and the migration of galaxy morphologies toward earlier Hubble types in rich and dense environments (see Boselli & Gavazzi 2006; Blanton & Moustakas 2009; Fumagalli & Gavazzi 2008), it has far more severe consequences for their nuclear regions. We are not yet in the position to distinguish these two effects. However, we are in the process of obtaining a complete set of Hα imaging follow-up observations of the Coma supercluster that is appropriate for distinguishing the nuclear from the extended star-formation in galaxies in this representative part of the local Universe.

Acknowledgements. G. Gavazzi wishes to thank his first year master students who assisted during the observing nights at Loiano for many years. We also thank R. Gualandi and all night assistants of the Loiano Observatory, and the coordinator of the TAC, V. Zitelli for the generous time allocation. We thank O. Cucciati for computing the local galaxy density parameter. We are grateful to P. Franzetti and A. Donati for their contribution to GoldMine, the Galaxy On Line Database extensively used in this work (http://goldmine.mib.infn.it). We acknowledge the constructive criticism from an anonymous referee.
The present study could not have been conceived without the DR7 of SDSS. Funding for the SDSS and SDSS-II has been provided by the Alfred P. Sloan Foundation, the Participating Institutions, the National Science Foundation, the US Department of Energy, the National Aeronautics and Space Administration, the Japanese Monbukagakusho, and the Max Planck Society, and the Higher Education Funding Council for England. The SDSS Web site is http://www.sdss.org/. The SDSS is managed by the Astrophysical Research Consortium (ARC) for the Participating Institutions. The Participating Institutions are the American Museum of Natural History, Astrophysical Institute Potsdam, University of Basel, University of Cambridge, Case Western Reserve University, The University of Chicago, Drexel University, Fermilab, the Institute for Advanced Study, the Japan Participation Group, The Johns Hopkins University, the Joint Institute for Nuclear Astrophysics, the Kavli Institute for Particle Astrophysics and Cosmology, the Korean Scientist Group, the Chinese Academy of Sciences (LAMOST), Los Alamos National Laboratory, the Max-Planck-Institute for Astronomy (MPIA), the Max-Planck-Institute for Astrophysics (MPA), New Mexico State University, Ohio State University, University of Pittsburgh, University of Portsmouth, Princeton University, the United States Naval Observatory, and the University of Washington. G. Gavazzi acknowledges financial support from Italian MIUR PRIN contract 200854ECE5.

References

Abazajian, K. N., Adelman-McCarthy, J. K., Agüeros, M. A., et al. 2009, ApJS, 182, 543
Baldwin, J. A., Phillips, M. M., & Terlevich, R. 1981, PASP, 93, 5

Binette, L., Magris, C. G., Stasińska, G., & Bruzual, A. G. 1994, A&A, 292, 13
Blanton, M. R., & Moustakas, J. 2009, ARA&A, 47, 159
Blanton, M. R., Schlegel, D. J., Strauss, M. A., et al. 2005a, AJ, 129, 2562
Blanton, M. R., Lupton, R. H., Schlegel, D. J., et al. 2005b, ApJ, 631, 208
Blanton, M. R., Eisenstein, D., Hogg, D. W., Schlegel, D. J., & Brinkmann, J. 2005c, ApJ, 629, 143
Boselli, A., & Gavazzi, G. 2006, PASP, 118, 517
Capetti, A., & Baldi, R. D. 2011, A&A, 529, A126
Cid Fernandes, R., Stasińska, G., Schlickmann, M. S., et al. 2010, MNRAS, 403, 1036
Cid Fernandes, R., Stasińska, G., Mateus, A., & Vale Asari, N. 2011, MNRAS, 413, 1687
Cortese, L., Gavazzi, G., & Boselli, A. 2008, MNRAS, 390, 1282
Cowie, L. L., Songaila, A., Hu, E. M., & Cohen, J. G. 1996, AJ, 112, 839
Crane, P., Peletier, R., Baxter, D., et al. 1993, ApJ, 402, L37
Decarli, R., Gavazzi, G., Arosio, I. et al. 2007, MNRAS, 381, 136
Dressler, A. 1980, ApJ, 236, 351
Dressler, A., Thompson, I. B., & Shectman, S. A. 1985, ApJ, 288, 481
Fontanot, F., De Lucia, G., Monaco, P., Somerville, R. S., & Santini, P. 2009, MNRAS, 397, 1776
Fumagalli, M., & Gavazzi, G. 2008, A&A, 490, 571
Gavazzi, G., & Perola, G. C. 1980, A&A, 84, 228
Gavazzi, G., Perola, G. C., & Jaffe, W. 1981, A&A, 103, 35
Gavazzi, G., Pierini, D., & Boselli, A. 1996, A&A, 312, 397
Gavazzi, G., Boselli, A., Donati, A., Franzetti, P., & Scodeggio, M. 2003, A&A, 400, 451
Gavazzi, G., Fumagalli, M., Cucciati, O., & Boselli, A. 2010, A&A, 517, A73
Giovanelli, R., Haynes, M. P., Kent, B. R., et al. 2005, AJ, 130, 2598
Hao, L., Strauss, M. A., Tremonti, C. A., et al. 2005, AJ, 129, 1783
Ho, L. C., Filippenko, A. V., & Sargent, W. L. W. 1997, ApJS, 112, 315
Kauffmann, G., Heckman, T. M., Tremonti, C., et al. 2003, MNRAS, 346, 1055
Kauffmann, G., White, S. D. M., Heckman, T. M., et al. 2004, MNRAS, 353, 713
Macchetto, F., Pastoriza, M., Caon, N., et al. 1996, A&AS, 120, 463
Mahajan, S., Haines, C. P., & Raychaudhury, S. 2010, MNRAS, 404, 1745
Miller, C. J., Nichol, R. C., Gómez, P. L., Hopkins, A. M., & Bernardi, M. 2003, ApJ, 597, 142
Panessa, F., & Bassani, L. 2002, A&A, 394, 435
Popesso, P., & Biviano, A. 2006, A&A, 460, L23
Sarzi, M., Shields, J. C., Schawinski, K., et al. 2010, MNRAS, 402, 2187
Schawinski, K., Virani, S., Simmons, B., et al. 2009, ApJ, 692, L19
Shen, Y., Mulchaey, J. S., Raychaudhury, S., Rasmussen, J., & Ponman, T. J. 2007, ApJ, 654, L115
Stasińska, G., Vale Asari, N., Cid Fernandes, R., et al. 2008, MNRAS, 391, L29
Strauss, M. A., Weinberg, D. H., Lupton, R. H., et al. 2002, AJ, 124, 1810
Trinchieri, G., & di Serego Alighieri, S. 1991, AJ, 101, 1647
Véron-Cetty, M.-P., & Véron, P. 2006, A&A, 455, 773
von der Linden, A., Wild, V., Kauffmann, G., White, S. D. M., & Weinmann, S. 2010, MNRAS, 404, 1231
Zwicky, F., Herzog, E., & Wild, P. 1961–68, Pasadena: California Institute of Technology (CIT)

Pages 12 to 16 are available in the electronic edition of the journal at http://www.aanda.org

Table 4. Parameters of 283 galaxies observed at Loiano.

Gal	RA	Dec	z	EWHα	EW[NII2]	Class	Avsp.	Activity
	J2000	J20000		Å	Å			
(1)	(2)	(3)	(4)	(5)	(6)	(7)	(8)	(9)
CGCG522-004	01:47:16.2	+35:33:48	0.01559	-0.554	-2.798	LIN	-	-
CGCG522-093	01:58:35.2	+38:43:07	0.01687	-9.228	-5.839	sAGN	-	-
CGCG522-104	02:00:59.7	+38:47:05	0.01888	-13.23	-7.936	sAGN	-	-
CGCG522-106	02:03:44.8	+38:15:31	0.01922	-3.166	-2.952	LIN	-	-
NGC 0891	02:22:33.4	+42:20:57	0.00176	-35.99	-15.06	HII	NED	-
NGC 0925	02:27:16.9	+33:34:45	0.00184	-35.87	-8.241	HII	NED	-
UGC01935	02:28:14.5	+31:18:42	0.01665	-144.8	-10.65	SY1	-	Sey1
NGC 1068	02:42:40.7	-00:00:48	0.00379	-81.52	-150.9	SY1	NED	Sey2
UGC02855	03:48:20.7	+70:07:58	0.00400	-23.25	-11.18	HII	-	-
NGC 1507	04:04:27.2	-02:11:19	0.00287	-82.32	-9.657	HII	-	-
NGC 1637	04:41:28.2	-02:51:29	0.00239	-37.04	-23.09	sAGN	-	-
NGC 1961	05:42:04.6	+69:22:42	0.01312	-10.06	-19.17	sAGN	NED	LINER
NGC 2273	06:50:08.7	+60:50:45	0.00613	-30.16	-28.54	SY1	NED	Sey2
NGC 2339	07:08:20.5	+18:46:49	0.00735	-37.87	-28.26	sAGN	NED	-
UGC03809	07:27:04.1	+80:10:41	0.00735	0.910	-1.431	RET	NED	-
NGC 2366	07:28:54.7	+69:12:57	0.00026	-2339	-20.87	HII	NED	-
NGC 2403	07:36:51.4	+65:36:09	0.00043	-0.97	-1.402	LIN	NED	-
NGC 2460	07:56:52.3	+60:20:58	0.00481	-7.404	-4.505	sAGN	-	-
NGC 2500	08:01:53.2	+50:44:14	0.00168	-1.484	-0.099	HII	NED	-
NGC 2537	08:13:14.6	+45:59:23	0.00143	-3.606	-2.357	HII	-	HII
UGC04278	08:13:58.9	+45:44:32	0.00180	-129	-10	HII	SDSS	-
CGCG119-016	08:14:14.2	+21:21:20	0.01129	-0.319	-2.227	LIN	-	-
CGCG119-029	08:17:25.8	+21:41:08	0.01189	-9.690	-5.93	sAGN	-	-
CGCG119-035	08:17:56.8	+22:26:08	0.00699	-53.40	-6.424	HII	SDSS	-
NGC 2549	08:18:58.4	+57:48:11	0.00346	1.885	-0.449	PAS	NED	-
CGCG119-055	08:19:38.0	+21:06:51	0.01882	-25.72	-23.6	sAGN	-	-
CGCG119-056	08:19:41.3	+22:02:31	0.01151	-48.29	-9.248	HII	SDSS	-
CGCG119-057	08:19:48.3	+22:01:53	0.01194	1.481	-1.812	RET	-	-
CGCG119-066	08:20:49.3	+22:39:28	0.01381	-21.90	-8.39	HII	SDSS	-
CGCG119-085	08:24:20.2	+20:32:00	0.01991	-9.358	-9.075	sAGN	SDSS	-
CGCG119-096	08:26:29.2	+22:15:40	0.02834	-39.12	-14.07	HII	SDSS	-
CGCG119-109	08:27:41.0	+21:28:47	0.01447	-6.181	-3.601	HII	-	-
NGC 2648	08:42:39.8	+14:17:08	0.00687	0.6825	-2.224	RET	-	-
NGC 2654	08:49:11.9	+60:13:16	0.00449	0.0	-1.235	RET	SDSS	-
NGC 2683	08:52:41.3	+33:25:18	0.00137	-1.439	-2.763	LIN	NED	-
NGC 2685	08:55:34.7	+58:44:04	0.00294	0.742	-1.323	RET	NED	Sey2
UGC4881S	09:15:54.0	+44:19:49	0.03948	-36.35	-19.07	sAGN	-	-
UGC4881N	09:15:55.0	+44:19:58	0.03974	-24.8	-15.72	sAGN	-	-
NGC 2841	09:22:02.6	+50:58:35	0.00212	-1.045	-3.727	LIN	NED	LINER
NGC 2903	09:32:10.1	+21:30:03	0.00185	-52.78	-19.8	HII	NED	-
NGC 3031	09:55:33.2	+69:03:55	-0.0001	-3.207	-6.37	LIN	NED	-
NGC 3115	10:05:14.0	-07:43:07	0.00221	0.0	0.0	PAS	NED	-
CGCG123-035	10:17:39.7	+22:48:36	0.00391	-10.12	-4.748	HII	-	-
CGCG124-003	10:20:38.0	+25:30:17	0.02002	0.923	0.0	PAS	-	-
IC0610	10:26:28.4	+20:13:41	0.00390	-6.495	-2.79	HII	-	-
CGCG124-033	10:31:18.7	+25:51:13	0.01950	3.353	0.0	PAS	-	-
NGC 3287	10:34:47.3	+21:38:54	0.00435	-16.56	-7.103	HII	SDSS	-
CGCG154-030	10:36:16.0	+26:57:43	0.02134	1.563	0.0	PAS	-	-
CGCG125-004	10:45:32.3	+24:09:00	0.02043	-7.33	-4.148	HII	-	-
CGCG155-023	10:50:22.7	+26:44:06	0.02168	-11.81	-3.975	HII	-	-
NGC 3412	10:50:53.3	+13:24:44	0.00280	1.67	0.0	PAS	NED	-
NGC 3424	10:51:46.3	+32:54:03	0.00498	-19.56	-13.84	sAGN	SDSS	-
NGC 3437	10:52:35.7	+22:56:03	0.00428	-27.35	-11.03	HII	SDSS	-
CGCG155-035	10:54:20.9	+27:14:23	0.00445	-7.90	-2.866	HII	-	-
NGC 3457	10:54:48.6	+17:37:16	0.00386	1.389	-1.007	RET	-	-
105825+241335	10:58:25.2	+24:13:35	0.02145	-1.527	-3.268	LIN	-	-
NGC 3485	11:00:02.4	+14:50:30	0.00479	-10.05	-5.731	sAGN	-	-
110127+274310	11:01:27.8	+27:43:10	0.02970	2.37	-3.39	RET	-	-
CGCG267-037	11:03:11.0	+56:13:18	0.00507	0.848	-0.912	RET	-	-
NGC 3512	11:04:02.9	+28:02:13	0.00459	-1.319	-2.938	LIN	SDSS	-
CGCG155-060	11:05:24.0	+26:21:53	0.02199	0.906	-0.745	RET	-	-
CGCG125-036	11:09:54.5	+24:15:25	0.02097	-56.82	-17.04	HII	-	-
NGC 3596	11:15:06.2	+14:47:13	0.00397	-13.7	-6.386	HII	NED	-
NGC 3599	11:15:27.0	+18:06:37	0.00277	-0.315	-1.2	LIN	-	-

Table 4. continued.

Gal	RA	Dec	z	EWHα	EW[NII2]	Class	Avsp.	Activity
	J2000	J20000		Å	Å			
(1)	(2)	(3)	(4)	(5)	(6)	(7)	(8)	(9)
CGCG096-038	11:23:45.5	+17:49:07	0.00428	-30.55	-9.221	HII	-	-
NGC 3657	11:23:55.6	+52:55:16	0.00405	-4.844	-2.347	HII	-	-
NGC 3683	11:27:31.8	+56:52:37	0.00572	-9.177	-3.803	HII	SDSS	-
CGCG126-070	11:29:51.0	+24:56:16	0.02515	-2.233	-1.356	HII	-	-
113220+223748	11:32:20.0	+22:37:48	0.03049	-25.87	-10.59	HII	-	-
113507+201303	11:35:07.0	+20:13:03	0.03119	-15.68	-10.2	sAGN	-	-
NGC 3758E	11:36:29.0	+21:35:45	0.02850	-186.9	12.08	SY1	-	-
NGC 3758W	11:36:29.0	+21:35:45	0.02948	-22.31	-13.09	sAGN	-	-
CGCG097-023	11:36:51.0	+20:00:17	0.02110	1.611	0.0	PAS	-	-
CGCG097-026	11:36:54.4	+19:58:15	0.02064	-46.71	-18.09	HII	-	-
CGCG127-006	11:37:43.0	+22:00:34	0.02982	1.574	-1.428	RET	-	-
CGCG127-007	11:37:49.0	+22:01:33	0.03029	1.022	-2.654	RET	-	-
CGCG127-012S	11:37:53.7	+21:58:51	0.02911	-1.472	-2.095	LIN	-	-
NGC 3773	11:38:12.9	+12:06:43	0.00327	-91.57	-15.93	HII	NED	Starb
FGC1287	11:39:11.0	+19:35:09	0.02279	-13.49	-6.852	HII	-	-
CGCG097-044	11:39:47.5	+19:56:00	0.03646	-5.509	-6.402	sAGN	-	-
113959+200935	11:39:59.0	+20:09:35	0.02395	0.906	0.0	PAS	-	-
CGCG157-012	11:40:39.0	+28:51:39	0.02287	-17.85	-5.929	HII	-	-
CGCG127-025S	11:40:44.2	+22:25:46	0.02360	-29.48	-13.64	HII	-	-
CGCG127-025N	11:40:44.6	+22:26:49	0.02353	-39.82	-19.58	HII	SDSS	-
CGCG127-032	11:42:09.1	+20:18:56	0.01922	1.214	-1.466	RET	-	-
UGC06678	11:43:01.9	+26:15:30	0.03161	1.375	-0.580	RET	SDSS	-
GCG097-082	11:43:24.6	+19:44:59	0.02034	2.273	0.0	PAS	-	-
CGCG097-092	11:43:58.2	+20:11:06	0.02125	-77.24	-21.96	HII	-	-
CGCG097-091	11:43:59.0	+20:04:37	0.02459	-20.28	-6.339	HII	SDSS	-
CGCG097-102N	11:44:17.2	+20:13:24	0.02124	0.0	0.0	PAS	-	-
CGCG097-121	11:44:47.0	+20:07:30	0.02195	-0.962	-2.665	LIN	-	-
CGCG097-114	11:44:47.8	+19:46:24	0.02766	-55.38	-16.19	HII	SDSS	-
114448+194828	11:44:48.9	+19:48:28	0.06770	-18.78	-8.65	HII	SDSS	-
CGCG097-120	11:44:49.2	+19:47:42	0.01866	-9.627	-6.969	sAGN	-	-
CGCG097-122	11:44:52.2	+19:27:15	0.01823	-31.86	-11.2	HII	-	-
CGCG097-128	11:45:03.9	+19:37:14	0.02171	0.0	0.0	PAS	-	-
CGCG097-127	11:45:05.0	+19:36:23	0.02171	-0.370	-2.569	LIN	SDSS	AGN
CGCG097-129E	11:45:07.0	+19:58:01	0.02517	-5.977	-6.482	sAGN	-	-
CGCG097-130	11:45:15.0	-19:23:31	0.02230	0.0	0.0	PAS	-	-
CGCG097-133E	11:45:17.6	+20:01:10	0.04845	-23.34	-8.531	HII	-	-
CGCG097-134	11:45:30.0	+19:24:00	0.02483	1.966	0.0	PAS	-	-
CGCG097-139	11:45:49.5	+19:46:03	0.02320	0.0	0.0	PAS	-	-
CGCG127-051N	11:45:59.4	+20:26:49	0.02370	-26.34	-11.14	HII	-	-
CGCG127-051S	11:45:59.9	+20:26:20	0.02438	-35.2	-17.33	HII	-	-
CGCG127-054	11:46:47.2	+20:40:32	0.02343	0.0	-2.258	RET	SDSS	-
114658+194444	11:46:58.0	+19:44:44	0.02073	1.345	-1.358	RET	-	-
CGCG157-032	11:47:07.9	+29:34:39	0.02271	0.0	0.0	PAS	SDSS	-
CGCG097-152	11:47:39.3	+19:56:22	0.02059	0.0	0.0	PAS	SDSS	-
CGCG157-035	11:48:03.4	+30:21:34	0.02101	-10.54	-4.672	HII	SDSS	-
114845+293828	11:48:45.0	+29:38:28	0.02237	-8.484	-11.03	SY1	-	-
CGCG127-063	11:49:59.3	+21:20:01	0.02624	0.5	-0.73	RET	-	-
CGCG127-073	11:51:02.3	+20:47:59	0.02143	0.500	-1.658	RET	-	-
CGCG127-075	11:51:21.0	+21:53:21	0.02648	0.0	0.0	PAS	-	-
CGCG127-076W	11:51:26.6	+22:01:41	0.02834	1.401	0.0	PAS	-	-
CGCG127-076E	11:51:28.2	+22:01:33	0.02566	0.0	0.0	PAS	-	-
CGCG157-045N	11:51:32.1	+27:38:49	0.02891	0.0	0.0	PAS	SDSS	-
CGCG157-045S	11:51:34.9	+27:38:23	0.02901	0.0	0.0	PAS	-	-
CGCG127-086	11:52:36.0	+23:34:55	0.02289	0.920	0.0	PAS	-	-
CGCG127-089	11:52:46.0	+20:59:20	0.02087	1.309	0.0	PAS	-	-
CGCG127-092	11:53:10.0	+20:39:28	0.02333	-1.583	-6.848	LIN	-	-
CGCG127-094	11:53:17.0	+23:27:52	0.02479	-27.27	-9.082	HII	-	-
115348+250912	11:53:48.1	+25:09:12	0.02837	-28.09	-12.18	HII	-	-
CGCG127-101	11:53:57.5	+25:41:06	0.01272	1.595	0.0	PAS	-	-
CGCG127-110	11:57:20.9	+25:11:43	0.01501	-2.286	-2.163	LIN	-	-
CGCG127-114W	11:57:48.2	+25:16:14	0.01591	-75.52	-18.87	HII	SDSS	-

Table 4. continued.

Gal	RA J2000	Dec J20000	z	EWHα Å	EW[NII2] Å	Class	Av.sp.	Activity
(1)	(2)	(3)	(4)	(5)	(6)	(7)	(8)	(9)
CGCG127-114E	11:57:50.0	+25:16:14	0.01591	-36.81	-9.359	HII	-	-
CGCG157-064	11:57:51.0	+29:02:20	0.02156	-41.94	-14.21	HII	-	-
CGCG127-116	11:57:59.0	+23:12:03	0.02370	0.446	-0.693	RET	-	-
CGCG157-065	11:58:05.2	+27:52:44	0.01123	-166.0	-31.74	HII	NED+SDSS	-
CGCG157-067	11:58:20.7	+28:21:35	0.02827	0.0	0.0	PAS	-	-
CGCG127-122	11:58:42.9	+25:02:25	0.01457	0.7803	-1.702	RET	-	-
CGCG127-130	11:59:36.0	+21:14:49	0.02635	0.136	-1.189	RET	-	-
NGC 4031	12:00:31.0	+31:56:51	0.02607	-21.34	-9.448	HII	-	-
CGCG127-134	12:01:12.0	+22:37:01	0.02761	-17.94	-5.692	HII	-	-
CGCG013-046	12:02:42.2	+01:58:37	0.00659	-13.95	-9.624	sAGN	NED+SDSS	-
CGCG098-030	12:02:50.2	+18:00:56	0.01605	-46.66	-18.55	HII	-	-
CGCG128-003	12:03:27.0	+22:12:36	0.02160	-27.95	-9.976	HII	-	-
NGC 4067	12:04:11.5	+10:51:16	0.00805	-0.269	-1.121	LIN	-	-
CGCG098-046	12:04:32.5	+20:12:18	0.02072	-0.974	-4.754	LIN	SDSS	-
CGCG098-058	12:07:03.5	+18:31:54	0.02404	0.0	-3.099	RET	SDSS	-
CGCG041-041	12:07:37.2	+02:41:26	0.00436	-82.8	-20.54	HII	-	-
CGCG041-042	12:08:11.1	+02:52:42	0.00442	-113.2	-60.62	sAGN	NED+SDSS	Starb
CGCG128-038	12:08:15.3	+25:48:41	0.02234	0.0	0.0	PAS	-	-
CGCG098-074	12:09:58.0	+19:55:04	0.02580	-14.88	-8.004	HII	-	-
CGCG158-036	12:10:18.3	+26:25:51	0.02174	0.0	0.0	PAS	SDSS	-
CGCG158-039	12:11:31.0	+29:05:20	0.02625	1.097	0.0	PAS	-	-
CGCG128-051	12:11:52.5	+24:07:25	0.00856	-9.625	-6.584	sAGN	NED	-
VCC0073	12:13:03.0	+07:02:20	0.00699	-2.612	-6.949	LIN	-	-
VCC0092	12:13:48.3	+14:54:01	-0.0004	-3.916	-5.802	LIN	NED	LINER
VCC0097	12:13:53.6	+13:10:22	0.00827	-14.82	-8.86	sAGN	SDSS	-
VCC0099	12:14:02.2	+06:43:24	0.00815	-5.344	-2.127	HII	SDSS	-
VCC0120	12:14:38.6	+05:48:21	0.00688	-29.58	-9.817	HII	-	-
CGCG158-055	12:15:59.2	+27:26:32	0.02551	-12.9	-7.803	sAGN	-	-
VCC0199	12:16:33.8	+07:27:44	0.00868	0.0	0.0	PAS	SDSS	-
VCC0362	12:19:42.3	+05:32:18	0.00512	-1.673	-2.282	LIN	-	-
VCC0382	12:19:56.1	+05:20:36	0.00793	-74.39	-26.45	HII	NED	-
NGC 4287	12:20:48.5	+05:38:24	0.00718	-22.1	-8.184	HII	-	-
CGCG158-084	12:21:01.0	+27:53:52	0.02480	0.0	0.0	PAS	-	-
VCC0449	12:21:02.3	+03:43:20	0.00873	-3.824	-1.758	HII	-	-
VCC0492	12:21:41.5	+05:23:05	0.00770	-3.436	-3.098	LIN	SDSS	-
CGCG128-082	12:21:45.6	+25:53:05	0.02304	0.0	-2.268	RET	SDSS-corr	-
VCC0562	12:22:35.9	+12:09:29	0.00014	0.0	0.0	PAS	SDSS	-
VCC0567	12:22:39.0	+06:40:37	0.00788	-19.05	-1.218	HII	SDSS	-
VCC0656	12:23:38.7	+06:57:15	0.00338	-1.838	-1.939	LIN	SDSS	-
VCC0697	12:24:05.5	+07:02:29	0.00410	-15.52	-5.061	HII	SDSS	-
VCC0792	12:25:22.2	+10:01:01	0.00321	-1.133	-1.827	LIN	NED+SDSS	-
CGCG158-106	12:26:19.9	+26:50:18	0.02361	0.0	0.0	PAS	-	-
VCC0912	12:26:32.2	+12:36:40	0.00034	-45.58	-14.27	HII	SDSS	-
VCC0958	12:26:56.4	+15:02:51	-0.0008	-3.428	-5.434	LIN	NED	-
CGCG128-089	12:26:59.5	+22:38:23	0.02281	0.441	-1.907	RET	SDSS	-
CGCG158-112	12:27:50.3	+26:59:37	0.02390	-4.337	-5.01	LIN	SDSS	-
CGCG159-002	12:28:15.4	+28:37:13	0.00220	-8.183	-4.646	HII	NED	-
VCC1110	12:28:29.6	+17:05:06	0.00651	-0.413	-3.252	LIN	NED	LINER
NGC 4460	12:28:45.6	+44:51:51	0.00163	-34.77	-7.781	HII	NED	-
VCC1145	12:28:59.0	+03:34:14	0.00294	-0.965	-3.249	LIN	NED	-
NGC 4490	12:30:36.2	+41:38:38	0.00188	-10.55	-2.92	HII	NED	-
VCC1330	12:30:59.7	+08:04:40	0.00580	1.616	-1.427	RET	-	-
CGCG159-010	12:31:38.6	+27:29:45	0.02337	-4.485	-1.948	HII	-	-
VCC1412	12:32:06.2	+11:10:35	0.00447	2.314	0.0	PAS	NED	-
CGCG014-062	12:32:28.2	+00:23:23	0.00503	-32.35	0.0	HII	NED+SDSS	-
VCC1442	12:32:36.5	+02:39:41	0.00576	-78.15	-9.636	HII	-	-
VCC1555	12:34:20.3	+08:11:52	0.00655	-46.91	-18.96	HII	NED	-
VCC1562	12:34:27.0	+02:11:17	0.00603	-33.47	-16.19	HII	NED	-
VCC1615	12:35:26.5	+14:29:47	0.00162	0.364	-2.348	RET	NED	LINER
CGCG159-024	12:35:57.6	+27:57:36	0.00269	-10.74	-5.087	HII	NED	-
CGCG129-011	12:36:30.3	+26:11:58	0.02377	2.246	-8.812	RET	-	-
VCC1690	12:36:49.8	+13:09:47	-0.0007	-5.7	-8.776	SY1	NED	Sey
CGCG159-033	12:37:21.1	+28:12:29	0.02559	0.0	-4.089	RET	SDSS	-

Table 4. continued.

Gal	RA	Dec	z	EWHα	EW[NII2]	Class	Av.sp.	Activity
	J2000	J20000		Å	Å			
(1)	(2)	(3)	(4)	(5)	(6)	(7)	(8)	(9)
VCC1727	12:37:43.5	+11:49:05	0.00506	-3.64	-11.27	SY1	NED	Sey2
VCC1757	12:38:17.9	+13:06:36	0.00593	-25.83	-6.683	HII	SDSS	-
CGCG159-043	12:39:18.0	+27:46:22	0.02185	0.711	-1.34	RET	-	-
CGCG159-045	12:39:18.0	+28:54:17	0.02490	1.626	-2.058	RET	-	-
IC3644	12:40:36.2	+26:30:17	0.02212	-13.98	-4.167	HII	-	-
IC3646	12:40:38.5	+26:31:34	0.02159	-38.46	-11.31	HII	-	-
CGCG159-053	12:41:08.0	+29:32:16	0.02330	0.0	-1.669	RET	-	-
NGC 4615	12:41:37.3	+26:04:22	0.01573	-33.99	-9.369	HII	-	-
NGC 4631	12:42:08.0	+32:32:29	0.00202	-124.2	-16.25	HII	NED+SDSS	-
VCC1923	12:42:31.1	+03:57:37	0.00245	-251.9	-70.92	HII	-	-
CGCG014-110	12:42:32.0	-00:04:57	0.00574	-36.21	-13.0	HII	-	-
CGCG129-020	12:42:54.0	+20:59:23	0.02182	-0.316	-2.462	LIN	-	-
CGCG100-005	12:44:53.1	+18:45:19	0.02205	-29.25	-16.64	sAGN	-	-
CGCG129-022	12:45:11.7	+23:02:09	0.02324	-0.295	-1.033	LIN	-	-
CGCG159-070	12:45:34.0	+27:03:35	0.02280	0.964	-0.707	RET	-	-
CGCG159-071	12:45:43.0	+29:25:58	0.02315	-34.99	-11.54	HII	-	-
124708+274736	12:47:08.5	+27:47:36	0.02485	-79.03	-16.24	HII	-	-
UGC7955	12:47:11.0	+26:42:48	0.02236	-8.625	-2.832	HII	-	-
CGCG100-007	12:47:11.4	+19:27:52	0.02264	2.037	-0.783	RET	-	-
VCC2070	12:48:22.9	+08:29:15	0.00336	-0.47	-2.432	LIN	NED	Sey2
CGCG129-025	12:49:34.2	+25:28:12	0.01462	-7.422	-2.434	HII	-	-
125209+272838	12:52:09.0	+27:28:38	0.01949	2.212	0.0	PAS	SDSS-corr	-
CGCG071-068	12:53:50.8	+09:42:36	0.00944	-56.73	-23.17	HII	SDSS	Starb
CGCG160-008	12:54:19.0	+27:04:05	0.02790	0.0	0.0	PAS	-	-
CGCG043-068	12:55:23.6	+07:54:34	0.00934	-18.77	-6.371	HII	-	-
CGCG160-021	12:56:12.1	+27:44:44	0.02306	0.0	0.0	PAS	-	-
CGCG160-025	12:56:27.9	+26:59:14	0.02155	-0.397	-3.658	LIN	SDSS	-
CGCG160-055	12:58:05.6	+28:14:34	0.02351	-86.04	-30.69	HII	SDSS	-
CGCG160-221	12:59:13.0	+27:58:37	0.02313	1.406	0.0	PAS	-	-
CGCG160-225	12:59:23.0	+27:54:39	0.02198	1.674	0.0	PAS	-	-
CGCG130-003	12:59:47.3	+21:48:48	0.02387	-23.69	-13.64	sAGN	SDSS	-
CGCG160-241	13:00:08.1	+27:58:37	0.02166	1.099	0.0	PAS	SDSS	-
CGCG160-248	13:00:17.7	+27:57:19	0.02302	0.0	-1.286	RET	-	-
CGCG043-093	13:00:39.1	+02:30:05	0.00320	-62.39	-20.17	HII	NED+SDSS	-
CGCG160-257	13:00:48.8	+28:09:30	0.01961	-0.434	-4.896	LIN	SDSS	-
CGCG160-258	13:00:51.0	+28:02:34	0.02867	1.495	0.0	PAS	-	-
CGCG015-055	13:00:58.7	-00:01:39	0.00396	-64.74	-20.66	HII	SDSS	Starb
CGCG160-261	13:00:59.3	+27:53:59	0.02300	2.189	0.0	PAS	-	-
CGCG160-096S	13:01:24.5	+29:18:30	0.02386	1.254	0.0	PAS	-	-
CGCG160-096N	13:01:25.3	+29:18:50	0.02316	-110.3	-77.82	SY1	SDSS	Sey2
CGCG160-095	13:01:26.1	+27:53:09	0.01828	-0.168	-3.555	RET	SDSS	-
CGCG160-102	13:01:43.4	+29:02:41	0.02366	-7.706	-5.815	sAGN	SDSS	-
CGCG160-121	13:03:29.1	+26:33:02	0.02226	-3.732	-2.039	HII	SDSS	-
CGCG130-005	13:04:10.8	+22:17:23	0.02386	-72.05	-39.34	sAGN	SDSS	-
130553+273307	13:05:53.1	+27:33:08	0.01888	1.296	0.0	PAS	-	-
CGCG160-154	13:10:20.0	+31:26:38	0.02540	3.687	-4.801	RET	-	-
CGCG160-163	13:12:59.4	+27:08:30	0.05972	-18.42	-13.12	sAGN	-	-
CGCG160-166	13:13:26.9	+27:48:09	0.02137	-0.428	-2.429	LIN	SDSS	-
CGCG130-021	13:13:45.3	+24:58:57	0.02418	-34.63	-15.94	HII	-	-
CGCG160-173	13:16:12.3	+30:57:01	0.01865	-8.16	-6.093	sAGN	-	-
CGCG160-177	13:16:51.0	+31:34:52	0.02980	-10.94	-5.381	HII	-	-
CGCG130-026	13:17:19.8	+20:38:17	0.02291	-10.64	-7.098	sAGN	SDSS	-
CGCG130-028	13:17:28.5	+20:36:44	0.02222	0.402	-2.198	RET	-	-
CGCG160-181	13:17:30.6	+31:05:34	0.01851	-15.01	-5.528	HII	-	-
CGCG160-182	13:17:45.2	+27:34:12	0.02332	-7.286	-4.848	sAGN	SDSS	-
CGCG160-198	13:20:01.0	+31:58:53	0.01813	0.0	0.0	PAS	-	-
CGCG160-200	13:20:14.0	+30:53:59	0.02448	-34.14	-15.18	HII	-	-
CGCG160-202	13:20:21.0	+31:30:53	0.01669	-10.55	-4.993	HII	-	-
NGC 5103	13:20:30.1	+43:05:02	0.00425	1.232	-0.522	RET	-	-
CGCG131-003	13:21:52.0	+22:25:45	0.03099	0.0	-1.675	RET	-	-
CGCG131-004	13:22:26.3	+21:25:33	0.02284	-42.45	-25.62	SY1	-	-
CGCG161-048	13:25:57.2	+31:37:06	0.02437	0.0	0.0	PAS	SDSS	-

Table 4. continued.

Gal	RA	Dec	z	EWHα	EW[NII2]	Class	Av.sp.	Activity
	J2000	J20000		Å	Å			
(1)	(2)	(3)	(4)	(5)	(6)	(7)	(8)	(9)
CGCG016-069	13:26:19.7	+02:06:03	0.00362	-4.201	-2.502	HII	NED	-
CGCG161-073	13:30:26.0	+31:37:15	0.02441	-0.306	-2.201	LIN	SDSS	-
135031+245834	13:50:31.0	+24:58:34	0.03041	1.048	-1.834	RET	-	-
CGCG132-023	13:51:05.4	+25:05:37	0.02923	0.0	0.0	PAS	-	-
135244+250223	13:52:44.0	+25:02:23	0.02857	1.11	0.0	PAS	-	-
NGC 5372	13:54:46.0	+58:40:01	0.00572	-66.55	-22.63	HII	-	-
CGCG132-047W	13:55:28.4	+25:04:25	0.02955	0.0	0.0	PAS	SDSS	-
CGCG132-047C	13:55:29.8	+25:04:25	0.02954	0.0	0.0	PAS	-	-
CGCG132-047E	13:55:32.6	+25:04:28	0.02850	0.0	0.0	PAS	-	-
CGCG132-058	13:57:15.4	+24:15:27	0.02965	-2.18	-1.045	HII	-	-
IC4397	14:17:58.7	+26:24:45	0.01474	-23.3	-8.77	HII	-	HII
141847+245625	14:18:47.0	+24:56:25	0.01766	-19.35	-9.173	HII	-	-
CGCG047-022	14:21:13.1	+03:26:09	0.00496	-6.435	-3.329	HII	-	-
CGCG133-055	14:26:17.7	+26:14:46	0.03024	-5.179	-4.07	sAGN	-	-
CGCG163-050	14:26:59.6	+26:51:50	0.03015	-10.65	-3.947	HII	-	-
142816+255055	14:28:16.0	+25:50:55	0.01457	0.770	0.0	RET	-	-
CGCG163-058	14:28:31.8	+27:24:32	0.01439	-3.236	-5.218	SY1	-	-
143409+275649	14:34:09.0	+27:56:49	0.03174	1.743	-1.857	RET	-	-
CGCG133-088	14:34:12.7	+25:28:05	0.01614	-11.72	-6.65	sAGN	-	-
CGCG163-085	14:35:01.9	+26:32:38	0.03070	-33.73	-12.09	HII	-	-
CGCG134-016	14:42:18.0	+25:30:34	0.02662	-3.055	-3.797	LIN	-	-
UGC9489S	14:43:01.0	+25:08:48	0.03083	-69.68	-10.7	HII	-	-
UGC9489N	14:43:02.0	+25:09:08	0.03088	-41.77	-33.8	sAGN	-	-
CGCG164-031	14:49:27.0	+27:46:51	0.03097	-0.877	-2.039	LIN	-	-
144954+274203	14:49:54.3	+27:42:03	0.02973	-30.69	-9.636	HII	-	-
CGCG134-054	14:54:44.8	+24:05:49	0.01732	-26.17	-9.219	HII	-	-
CGCG134-066	15:01:53.7	+25:57:52	0.02205	-2.708	-5.947	LIN	-	-
IC4530	15:03:45.0	+26:06:03	0.03121	-2.438	-2.079	LIN	-	-
CGCG165-021	15:08:01.0	+27:58:20	0.03196	0.767	-1.769	RET	-	-
NGC 5957	15:35:23.2	+12:02:51	0.00609	-1.279	-3.044	LIN	SDSS	-
CGCG136-042	15:39:27.4	+24:56:51	0.02291	-88.94	-52.51	sAGN	-	Starb
CGCG136-067	15:45:16.0	+24:37:50	0.02233	1.482	0.0	PAS	-	-
NGC 6166	16:28:38.5	+39:33:06	0.03035	-1.369	-7.51	LIN	-	-